

THE RELATIONSHIP OF MULTISPECTRAL SATELLITE IMAGERY TO IMMEDIATE FIRE EFFECTS

**Andrew T. Hudak^{1,*}, Penelope Morgan², Michael J. Bobbitt², Alistair M.S. Smith²,
Sarah A. Lewis¹, Leigh B. Lentile², Peter R. Robichaud¹, Jess T. Clark³
and Randy A. McKinley⁴**

¹Forest Service, U.S. Department of Agriculture,
Rocky Mountain Research Station, Moscow, Idaho

²University of Idaho, Department of Forest Resources, Moscow, Idaho

³RedCastle Resources, Inc., contractor to the Forest Service,
U.S. Department of Agriculture, Remote Sensing Applications Center,
Salt Lake City, Utah

⁴Science Applications International Corp., contractor to the U.S. Geological Survey,
Center for Earth Resources Observation and Science, Sioux Falls, South Dakota

*Corresponding author: Tel.: (208) 883-2327; e-mail: ahudak@fs.fed.us

ABSTRACT

The Forest Service Remote Sensing Applications Center (RSAC) and the U.S. Geological Survey Earth Resources Observation and Science (EROS) Data Center produce Burned Area Reflectance Classification (BARC) maps for use by Burned Area Emergency Response (BAER) teams in rapid response to wildfires. BAER teams desire maps indicative of fire effects on soils, but green and nonphotosynthetic vegetation and other materials also affect the spectral properties of post-fire imagery. Our objective was to assess how well satellite image-derived burn severity indices relate to a suite of immediate post-fire effects measured on the ground. We measured or calculated fire effects variables at 418 plots, nested in 50 field sites, located across the full range of burn severities observed at the 2003 Black Mountain, Cooney Ridge, Robert, and Wedge Canyon wildfires in western Montana, the 2003 Old and Simi wildfires in southern California, and the 2004 Porcupine and Chicken wildfires in interior Alaska. We generated the Normalized Burn Ratio (NBR), differenced Normalized Burn Ratio (dNBR), Relative dNBR (RdNBR), Normalized Difference Vegetation Index (NDVI), and differenced NDVI (dNDVI) burn severity indices from Landsat 5 Thematic Mapper (TM) imagery across these eight wildfires. The NBR correlated best with the fire effects measures but insignificantly, meaning other indices could act as suitable substitutes. The overstory (trees in Montana and Alaska, shrubs in California) measures appear to correlate best to the image variables, followed by understory and surface cover measures. Exposed mineral soil and soil water repellency were poorly correlated with the image variables, while green vegetation was most highly correlated. The BARC maps are more indicative of post-fire vegetation condition than soil condition. We conclude that the NBR and dNBR, from which BARC maps of large wildfires in the United States are currently derived, are sound choices for rapid assessment of immediate

post-fire burn severity across the three ecosystems sampled. Our future research will focus on spectral mixture analysis (SMA) because it acknowledges that pixel reflectance is fundamentally a mixture of charred, dead, green and nonphotosynthetic vegetation, soil, rock and ash materials that are highly variable at fine scales.

Keywords: burn severity, change detection, char, Landsat, normalized burn ratio, remote sensing, soils, spectral mixture analysis, vegetation, wildfire

Citation: Hudak, A.T., P. Morgan, M.J. Bobbitt, A.M.S. Smith, S.A. Lewis, L.B. Lentile, P.R. Robichaud, J.T. Clark and R.A. McKinley. 2007. The relationship of multispectral satellite imagery to immediate fire effects. *Fire Ecology* 3(1): 64-90.

INTRODUCTION

Large wildfires have occurred and will continue to occur often in ecosystems of the United States, especially the drier ecosystems of the western U.S. (Morgan *et al.* 2003). Wildfires are an essential component of these ecosystems, but have become increasingly expensive to suppress as human development expands the wildland-urban interface (WUI). The U.S. Forest Service and Department of Interior annually expend millions of dollars to suppress wildfires that endanger people or their property. Additional millions are spent by Burned Area Emergency Response (BAER) teams to rehabilitate recently burned areas, especially those severely burned and vulnerable to erosion, sedimentation of water supplies, or encroachment by undesirable invasive species. Efforts to increase the efficiency of post-fire rehabilitation treatments rely in large part on accurate maps of where severely burned areas occur across the landscape, along with their appropriate use in burn severity assessments.

Once a wildfire is contained, BAER teams have about one week to complete a post-fire rehabilitation plan. To expedite their work, BAER team leaders desire Burned Area Reflectance Classification (BARC) maps within a couple of days after arriving on an incident. BARC maps are produced as rapidly as possible by the Remote Sensing Applications Center (RSAC) on U.S. Forest Service (USFS)

managed lands, and U.S. Geological Survey (USGS) Center for Earth Resources Observation and Science (EROS) on Department of Interior managed lands. Landsat imagery is the default choice for mapping large and small fires key to local management needs (Clark *et al.* 2003), with moderate-resolution satellite sensors such as SPOT, ASTER, and others serving as supplementary sources of satellite imagery. The prevailing need to produce a BARC map quickly largely drives the choice of which satellite sensor to use.

BARC maps are so named to distinguish themselves from burn severity maps produced by BAER teams to identify areas where fire greatly impacted the soil. BARC maps are helpful to BAER teams as a preliminary indicator of soil erosion potential, which is their primary concern. The production of burn severity maps by BAER teams is essentially a field validation exercise that uses a variety of methods to determine appropriate thresholds for distinguishing severely burned areas from areas only moderately or lightly burned, as indicated in BARC maps. Lewis *et al.* (2007) describe the specific fire effects on soils that contribute to soil erosion potential.

BARC maps are derived from either the Normalized Burn Ratio (NBR) or differenced NBR (dNBR) indices (Key and Benson 2003, van Wagendonk *et al.* 2004). Although dNBR is the default choice as a burn severity indicator, Bobbe *et al.* (2003), in a field

validation of BARC maps, found dNBR to be no more accurate than NBR. They called for further assessments across a greater range of ecosystems, a need that prompted this study, which considered burn severity in terms of fire effects on both soil and vegetation.

Images from low spatial resolution satellite sensors such as MODIS, SPOT-VEG, and AVHRR have been widely used for regional measures of burned area (Barbosa *et al.* 1999, Stroppiana *et al.* 2002). Regional burned area products (e.g., GBA2000, GLOBSCAR, etc.) have been heavily evaluated (Gregoire *et al.* 2003), and there currently exists extensive literature that has investigated the application of remote sensing techniques to measure the area burned using a wide variety of satellite sensors at both moderate (Smith *et al.* 2002, Hudak and Brockett 2004) and broad scales (Barbosa *et al.* 1999, Zhang *et al.* 2003).

In contrast, the remote assessment of burn severity from aerial and satellite imagery remains relatively under researched (Lentile *et al.* 2006). Indeed, the relationships between spectral properties of burned areas and field measures of burn severity have been evaluated in few studies (Landmann 2003, van Wagtenonk *et al.* 2004, Smith *et al.* 2005, Lewis *et al.* 2006, Robichaud *et al.* 2007). The remote assessment of burn severity is expected to be highly dependent on the acquisition date of the image following the fire, as spectral evidence of charring or the quantity and character of the ash produced by the fire will be quickly altered by meteorological processes and vegetation regrowth (Robinson 1991). Therefore, the utility of NBR, dNBR, and other indices with potential for mapping burn severity needs to be quantitatively tested across a variety of image types and acquisition dates. Preferably, maps of specific fire effects (e.g., cover of exposed soil, organic matter, or vegetation) with biophysical relevance might be produced, instead of maps keyed using loose burn severity definitions that are less interpretable and useful (Lentile

et al. 2006), and may even run the risk of misinterpretation or misuse.

Our objective was to assess how well indices derived from Landsat Thematic Mapper (TM) imagery relate to a suite of immediate post-fire effects measured on the ground to characterize burn severity. We defined burn severity as the degree of ecological change resulting from the fire (Morgan *et al.* 2001, National Wildfire Coordination Group 2005, Lentile *et al.* 2006) and considered fire effects on both vegetation and soils. To obtain this information, we conducted an extensive field validation project at four wildfires in western Montana mixed-conifer forest, two in southern California chaparral, and two in interior Alaska boreal forest. Lentile *et al.* (2007) provide a detailed description of the vegetation and topographic characteristics of the areas sampled.

METHODS

Wildfires Sampled

We characterized fire effects across the full range of burn severity observed in the field, as soon as possible after eight large wildfire events in 2003 and 2004 (Figure 1). The Black Mountain and Cooney Ridge wildfires, located west and east of Missoula, Montana, respectively, together burned over 10,000 ha during much of August and into September, 2003. Beginning in mid-July and for the next two months, the Robert and Wedge Canyon wildfires west of Glacier National Park burned nearly 45,000 ha combined. In less than two weeks between late October and early November, 2003, the Old and Simi wildfires north of San Bernadino and Simi Valley, respectively, collectively burned over 80,000 ha in southern California. The largest 2004 wildfires in the United States were in interior Alaska, the largest of which was the Taylor Complex southeast of Fairbanks. The Porcupine and Chicken wildfires sampled in this project in late July expanded along with the

Wall Street, Billy Creek, and Gardiner Creek fires to merge eventually into the >520,000 ha Taylor Complex portrayed in Figure 1.

Before entering an active fire zone and upon leaving, we followed established safety protocols and communicated our location and intention with the Incident Command. The importance of strict adherence to wildfire safety procedures cannot be overemphasized (Lentile *et al.* 2007a, b). One advantage of our

rapid response research project was our ability to obtain fire progression records from the Incident Command GIS team, while on these active incidents. From these records, or by asking fire personnel who were on the ground at the time of burning, we established the burn dates for all of the plots we sampled. This later allowed us to calculate how soon after each plot burned the fire effects were characterized.

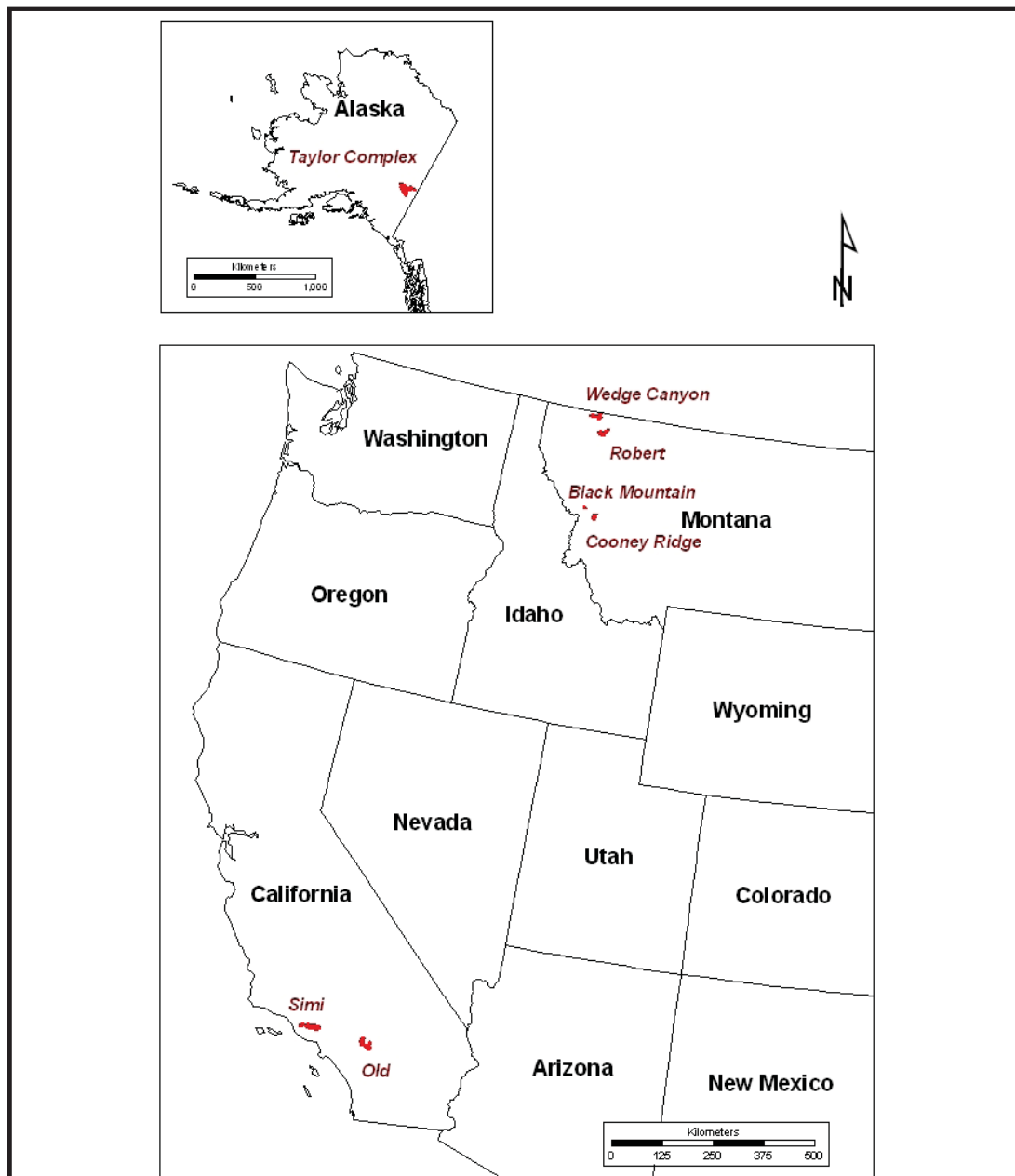


Figure 1. Eight wildfires sampled in western Montana, southern California, or interior Alaska.

Image Processing

The spectral channels, spatial resolution and coverage, temporal frequency, and low cost of Landsat TM make it the preferred image sensor for rapid production of BARC maps by RSAC and EROS. Satellite images are selected based on the availability of a cloud-free scene as soon as possible after the need for BARC maps is identified.

Most image data used in this analysis came from the Landsat 5 TM sensor (Table 1) because images could be obtained for all eight wildfires sampled, thus eliminating sensor type as a source of variation in the analysis. All the images were provided by either RSAC (Montana and California fires) or EROS (Alaska fires). Each was already rectified geometrically and radiometrically, and calibrated to top-of-atmosphere reflectance, following accepted preprocessing procedures (http://landcover.usgs.gov/pdf/image_preprocessing.pdf).

We calculated NBR (Equation 1) because it is the most applied burn severity index, together with its corresponding differenced index, differenced NBR (dNBR; Equation 2), developed by Key and Benson (2003). We

also assessed the Relative dNBR (RdNBR; Equation 3), which transforms the dNBR to a relative scale and can remove heteroscedasticity from the distribution of dNBR values, which improved burn severity classification accuracy in the Sierra Nevada of California (Miller and Thode 2007). In addition, we included the NDVI (Equation 4) because of its broad use in remote sensing across most satellite sensors, and the corresponding change index, differenced NDVI (dNDVI; Equation 5).

$$NBR = (NIR - SWIR) / (NIR + SWIR) \quad (1)$$

$$dNBR = NBR_{prefire} - NBR_{postfire} \quad (2)$$

$$RdNBR = (NBR_{prefire} - NBR_{postfire}) / \sqrt{(|NBR_{prefire}| / 1000)} \quad (3)$$

$$NDVI = (NIR - RED) / (NIR + RED) \quad (4)$$

$$dNDVI = NDVI_{prefire} - NDVI_{postfire} \quad (5)$$

In the above formulas, RED denotes the red band, Landsat band 3; NIR denotes the near infrared band, Landsat band 4; and SWIR denotes the short wave infrared band, Landsat band 7.

We also applied spectral mixture analysis (SMA) to the six reflectance bands of each

Table 1. Landsat 5 TM images used to characterize burn severity at eight wildfires.

Wildfire Sampled	Ignition Date	Containment Date	Pre-Fire Image Date	Pre-Fire Path/Row	Post-Fire Image Date	Post-Fire Path/Row
Black Mountain	8-Aug-03	14-Sep-03	10-Jul-02	P41/R27	25-Oct-03	P41/R27
Cooney Ridge	8-Aug-03	14-Sep-03	10-Jul-02	P41/R27	31-Aug-03	P40/R28
Robert	23-Jul-03	17-Sep-03	3-Oct-01	P41/R26	25-Oct-03	P41/R26
Wedge Canyon	18-Jul-03	13-Sep-03	3-Oct-01	P41/R26	25-Oct-03	P41/R26
Old	25-Oct-03	5-Nov-03	7-Oct-02	P40/R36	19-Nov-03	P40/R36
Simi	25-Oct-03	1-Nov-03	12-Sep-02	P41/R36	10-Nov-03	P41/R36
Porcupine	21-Jun-04	16-Sep-04 ¹	15-Sep-03	P65/R15-16	8-Sep-04	P66/R15
Chicken	15-Jun-04	16-Sep-04 ¹	15-Sep-03	P65/R15-16	8-Sep-04	P66/R15

¹Date of the last situation report mentioning the 2004 Alaska fires.

post-fire Landsat TM image to estimate green vegetation (green), nonphotosynthetic vegetation (brown), and char (black) fractional cover. SMA is an established remote sensing method that has been applied to both delineate areas burned and calculate the fractional cover of vegetation and char within burned pixels (Wessman *et al.* 1997, Cochrane and Souza 1998, Smith *et al.* 2007). In SMA, the solution of a linear model enables the calculation of the relative proportions that a given cover type contributes to pixel reflectance. The linear mixture model (Equation 6, Cochrane and Souza 1998) is defined by:

$$R_i = \sum_{j=1}^n (R_{i,j} f_j) + e_i \quad (6)$$

where R_i is the spectral reflectance of the i^{th} spectral band of a pixel; $R_{i,j}$ is the spectral reflectance of endmember j in band i ; f_j is the fraction of endmember j ; and e_i is the error in band i . Following Smith *et al.* (2007), generic spectral endmembers of green vegetation, nonphotosynthetic vegetation, and char (as presented in Smith *et al.* 2005) were used as these example spectra are broadly similar across most vegetation types (Elvidge 1990, Landmann 2003). The same generic endmembers were used for all of the fires in this analysis.

Pixel values from the five burn severity index images and three fractional cover images were extracted at the field subplot center point locations (i.e., 135 subplots per site; Figure 2). For simplicity throughout the remainder of this paper, we may refer to all eight image variables as indices, although strictly speaking fractional cover images are not indices but physically-based estimates.

Field Sampling

Fire effects data were collected 11 Sep to 13 Oct, 2003, at the Missoula fires in Montana; 29 Sep to 23 Oct, 2003, at the Glacier fires in Montana; 6 to 14 Dec, 2003, in California;

and 22 to 31 Jul, 2004, in Alaska. The goal for selecting field sites was to find burned areas with severity conditions that were large enough to include many Landsat image pixels and that were broadly representative of the range of post-fire conditions occurring across the post-fire landscape. When a desired burn severity condition that could be safely accessed was found, the center of the field site was placed a random distance away from and on a compass bearing perpendicular to the access road. While preliminary BARC maps were used as rough guides to navigate to burned areas of interest, field sites were considered as having low, moderate, or high severity if the tree crowns were predominantly green, brown, or black, respectively. This field assessment of burn severity class often did not agree with the class shown on the preliminary BARC map.

Each field site consisted of a systematic layout of nine plots, with 15 subplots further nested within each plot. Thus, a field site was designed to sample fine-scale variation in fire effects within a selected burn severity condition, while other field sites captured variation in fire effects between different burn severity conditions. The field site center was randomly located within a selected severity condition that was consistent in terms of observed fire effects and apparent pre-fire stand structure and composition; i.e., we had a rule that the field site should not be situated closer than a 30 m pixel distance to an obvious edge in the severity condition being sampled. The site center was designated the center of plot A, while the remaining eight plots were laid out systematic distances away, with the site oriented according to slope direction (Figure 2). The nine plots were intentionally spaced apart by unequal intervals of 20 m, 30 m, or 40 m to spread out the distribution of lag distances separating the observations. This was done to facilitate a more robust assessment of the spatial autocorrelation in fire effects that underlies observed patterns. Each plot was further

subdivided into fifteen 1 m x 1 m subplots arrayed in a 3 row x 5 column grid as depicted in Figure 2. The centers of plots A-I were all geolocated with a Global Positioning System (GPS), logging a minimum of 150 positions, which were later differentially corrected and averaged to decrease the uncertainty to <2 m. Horizontal distances between plot centers were measured using a laser rangefinder to

correct for slope effects. The centers of the other subplots were laid out using a cloth tape for distance and a compass for bearing, and marked with reusable pin flags. Subplot centers were not geolocated with the GPS, but their geolocations were later calculated based on their known systematic distance and bearing from the measured plot centers.

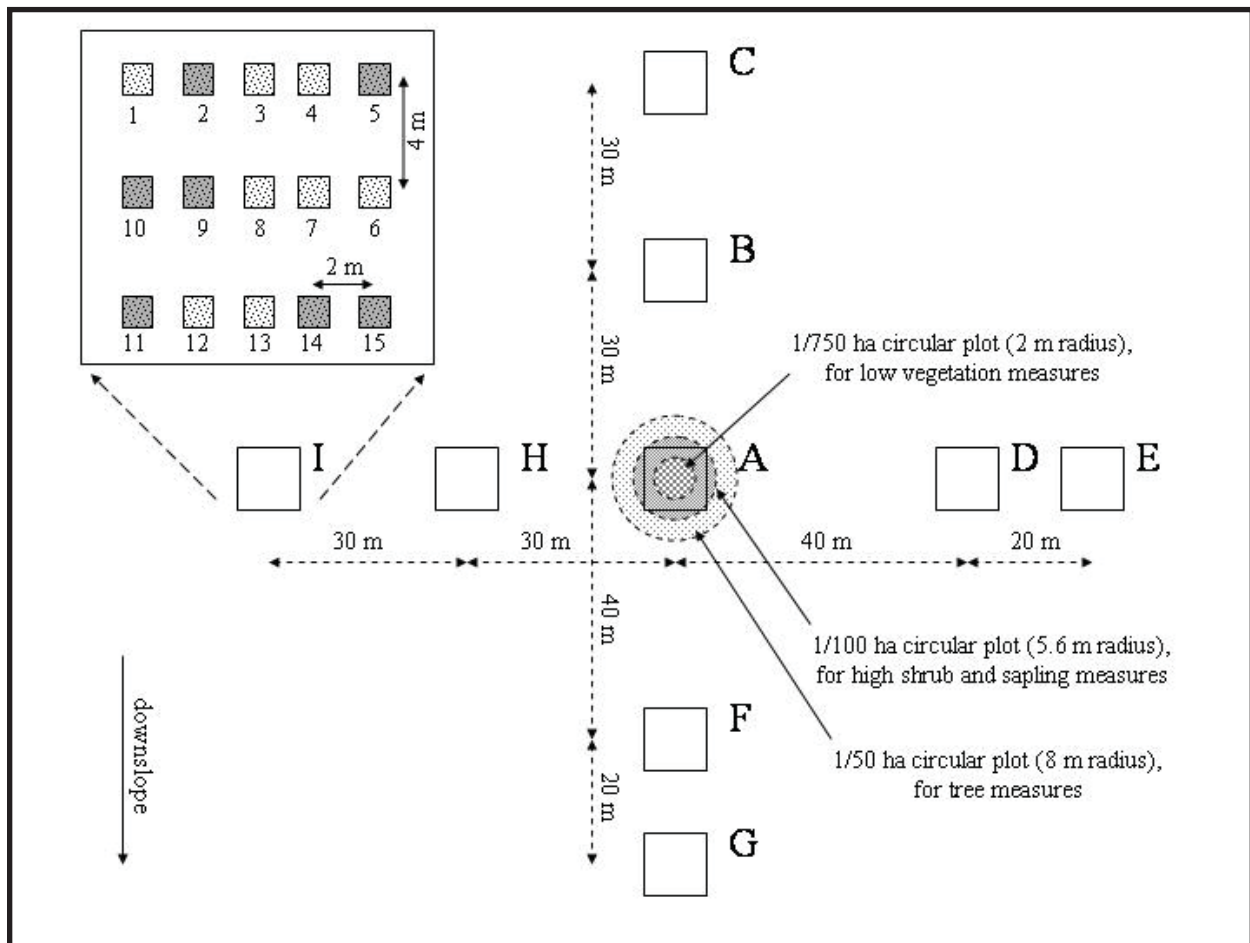


Figure 2. Systematic plot and subplot layout at a field site. Each field site was composed of nine 9 m x 9 m square plots (A-I), and each plot was composed of fifteen 1 m x 1 m square subplots (inset) for 9 x 15 = 135 subplots per site. Soil water repellency or duff moisture measures were conducted at the subset of subplots shown in gray. Vegetation composition was measured at the center of the field site in one of three circular subplots, depending on life form.

A suite of fire effects was measured at the subplot or plot scale at each field site (Table 2). At the subplot scale, surface cover fractions of green vegetation, rock, mineral soil, ash, litter, and any large surface organics were estimated ocularly, with the aid of a 1 m² square quadrat. Percent char of each unconsumed cover component was also recorded. A ruler was used to measure depth of new litter (deposited post-fire), old litter (existing pre fire), and duff. Old litter and duff depth were measured once per plot in Montana and California, and thrice per plot in Alaska because the deep duff layer is an important fuels component and determinant of fire behavior in the boreal forest. Also for this reason in Alaska, duff moisture was measured with a duff moisture meter (Robichaud *et al.* 2004). Water repellency of soils that were charred lightly (black), moderately (gray), deeply (orange), or were uncharred was measured using both a mini-disk infiltrometer (Robichaud in press) and a water drop penetration test (DeBano 1981). The water drop penetration test has been used more in the past, but the mini-disk infiltrometer is considered a superior measurement because it is volumetric while the water drop test is not (Lewis *et al.* 2006). Water repellency was measured in only 7 of the 15 subplots within each plot (Figure 2) to reduce the sampling effort. Water repellency was not measured at 19 of the 50 sites sampled because the soils were too wet after recent precipitation for reliable measurements. A convex spherical densiometer was used to measure canopy closure around the center subplot (subplot 8) facing the four cardinal directions. Topographic features were also recorded at every plot, along with a digital photograph for reference.

At every site, percent canopy cover of grasses, forbs, low shrubs (<1 m tall, or <1 cm basal diameter if the shrub was consumed to leave only a charred stub), and tree seedlings was estimated in a 1/750 ha circular plot; tall shrubs (>1 m tall, or >1 cm basal diameter if

the shrub was consumed to leave only a charred stub) and tree saplings were tallied in a 1/100 ha plot; and trees and snags (>12 cm dbh) were inventoried in a 1/50 ha plot. These three fixed-radius vegetation plots were arranged concentrically at site center (Figure 2). With the exception of canopy closure measured at every square plot, the other overstory and understory vegetation variables were only assessed in one of the circular plots centered over plot A of each site (Figure 2), and therefore constituted only 1/9 the sampling effort as the measures made at the 9 square plots A-I (Table 2).

Analysis

A number of variables in Table 2 were not measured directly in the field but calculated later. Total organic charred and uncharred cover fractions were derived by combining the charred and uncharred fractions of the old litter and other organic constituents (stumps, logs, etc.) estimated in the field. Total inorganic charred and uncharred cover fractions were similarly calculated by summing the charred and uncharred mineral soil and rock fractions estimated in the field. Water repellency measurements were weighted by the light, moderate, deep, and uncharred soil cover fractions they represented within the subplot sampled, then aggregated. The four canopy closure measurements made at each field plot with a convex spherical densiometer were rescaled from 0-96 canopy counts/measurement to 0% to 100%, as is standard with this instrument, and then averaged. Moss, liverwort, fern, forb, and low shrub cover estimates from the 1/750 ha center vegetation plot were summed to estimate total green (living), brown (scorched), or black (charred) understory cover. The number of dead seedling, sapling, high shrub, and tree stems was divided by the total number of living and dead stems tallied in the field to calculate percent mortality. Field estimates of the green, scorched, or charred proportions of

Table 2. Fire effects measured at a field site (Figure 2).

Stratum	Variable (units)	Measurement Scale
Overstory		
	overstory canopy closure (%)	plots A-I
	green tree crown (% green)	1/50 ha center plot
	scorched tree crown (% brown)	1/50 ha center plot
	charred tree crown (% black)	1/50 ha center plot
	tree mortality (% dead)	1/50 ha center plot
Understory		
	high shrub mortality (% dead)	1/100 ha center plot
	sapling mortality (% dead)	1/100 ha center plot
	seedling mortality (% dead)	1/750 ha center plot
	green understory cover (% green)	1/750 ha center plot
	scorched understory cover (% brown)	1/750 ha center plot
	charred understory cover (% black)	1/750 ha center plot
Surface		
	new litter cover fraction (%)	subplots 1-15
	old litter cover fraction (%)	subplots 1-15
	ash cover fraction (%)	subplots 1-15
	soil cover fraction (%)	subplots 1-15
	rock cover fraction (%)	subplots 1-15
	uncharred organic cover fraction (%)	subplots 1-15
	charred organic cover fraction (%)	subplots 1-15
	total organic cover fraction (%)	subplots 1-15
	uncharred inorganic cover fraction (%)	subplots 1-15
	charred inorganic cover fraction (%)	subplots 1-15
	total inorganic cover fraction (%)	subplots 1-15
	total green cover fraction (%)	subplots 1-15
	total uncharred cover fraction (%)	subplots 1-15
	total charred cover fraction (%)	subplots 1-15
Subsurface		
	new litter depth (mm)	plots A-I
	old litter depth (mm)	plots A-I
	duff depth (mm)	plots A-I
	duff moisture (%)	7 subplots / plot
	mini-disk infiltrometer rate (ml/min)	7 subplots / plot
	mini-disk infiltrometer time (s)	7 subplots / plot
	water drop penetration time (s)	7 subplots / plot

individual tree crowns were weighted by their crown length before averaging to represent the entire plot.

All of the eight image and 32 field variables were aggregated to the plot scale for this analysis. This was deemed necessary because the 2 m sampling interval between subplots was smaller than the positional uncertainty of the subplot locations. Also, not all variables were measured at the subplot scale, but all variables were measured at the plot scale (although not necessarily at every plot), and every plot position was geolocated with the GPS, making the plot scale most appropriate for this analysis of image-field data relationships. Correlation matrices between the image and field variables were generated in R (R Development Core Team, 2004), as were the boxplots and scatterplots that efficiently illustrate the highly variable relationships between the image and field variables.

RESULTS

Rapid Response

Each wildfire sampled was wholly contained within a single Landsat TM satellite path (Table 1), which simplified the image acquisition variable to a single date. Thus on every wildfire, the distribution of days elapsed between burn date and image acquisition date, or field characterization date and image acquisition date, was wholly a function of the fire progression or the speed at which we characterized the plots in the field, respectively (Figure 3). The California wildfires spread rapidly, driven by Santa Ana winds in predominantly chaparral vegetation. Fire progressions were typically slower in forests in Montana and Alaska, especially in Alaska where smoldering combustion in the deep duff can continue for months. The delay between when the field plots burned and when a cloud-free Landsat TM image was acquired ranged

from 0 to 97 days (Figure 3). In the case of the California and Montana fires (except Cooney Ridge), BAER teams needed BARC maps before a Landsat overpass, prompting RSAC to obtain images from other sensors.

The delay between when the plots burned and when they were characterized in the field ranged from 5 to 93 days (Figure 3). The longest field sampling delays were at the Robert and Wedge Canyon fires because we were unable to access these fires west of Glacier National Park until after our team had finished sampling the Black Mountain and Cooney Ridge fires near Missoula. The Missoula, Glacier, California, and Alaska wildfires are arranged top-bottom along the y-axes in Figure 3 by the order in which they were sampled. Generally, the speed of field work increased as the crews grew accustomed to the sampling protocol.

The dates of image acquisition and field plot characterization were fairly well balanced (Figure 3). The field plots at the Cooney Ridge and two California wildfires were imaged 19 to 43 days before we could reach them on the ground, while field plot sampling at the other five wildfires followed image acquisitions by 1 to 48 days (Figure 3).

We tested if any of the time lags between burning, image acquisition, and field characterization dates might confound the image-field data relationships of primary interest. Plot-level correlation matrices were generated between the eight image variables and the 14 surface cover fractions measured or calculated at all of the subplots. Of the 418 field plots sampled in this study, 117 had no variation in 30 m pixel values between the subplots, preventing calculation of correlation matrices within these. The median of the correlations (absolute values) for each of the remaining 301 plots was plotted against the three time lag variables to form three scatterplots, and smoothed loess functions were fit to these scatterplots to illustrate the trends (Figure 4). These trends were tested for significance, but

none were over the entire ranges of time lags shown. However, there is visibly a slight trend in days elapsed between field plot burning and

field plot characterization that was significant ($p = 0.0018$) based on 104 field plots characterized in the first 36 days after burning (Figure 4).

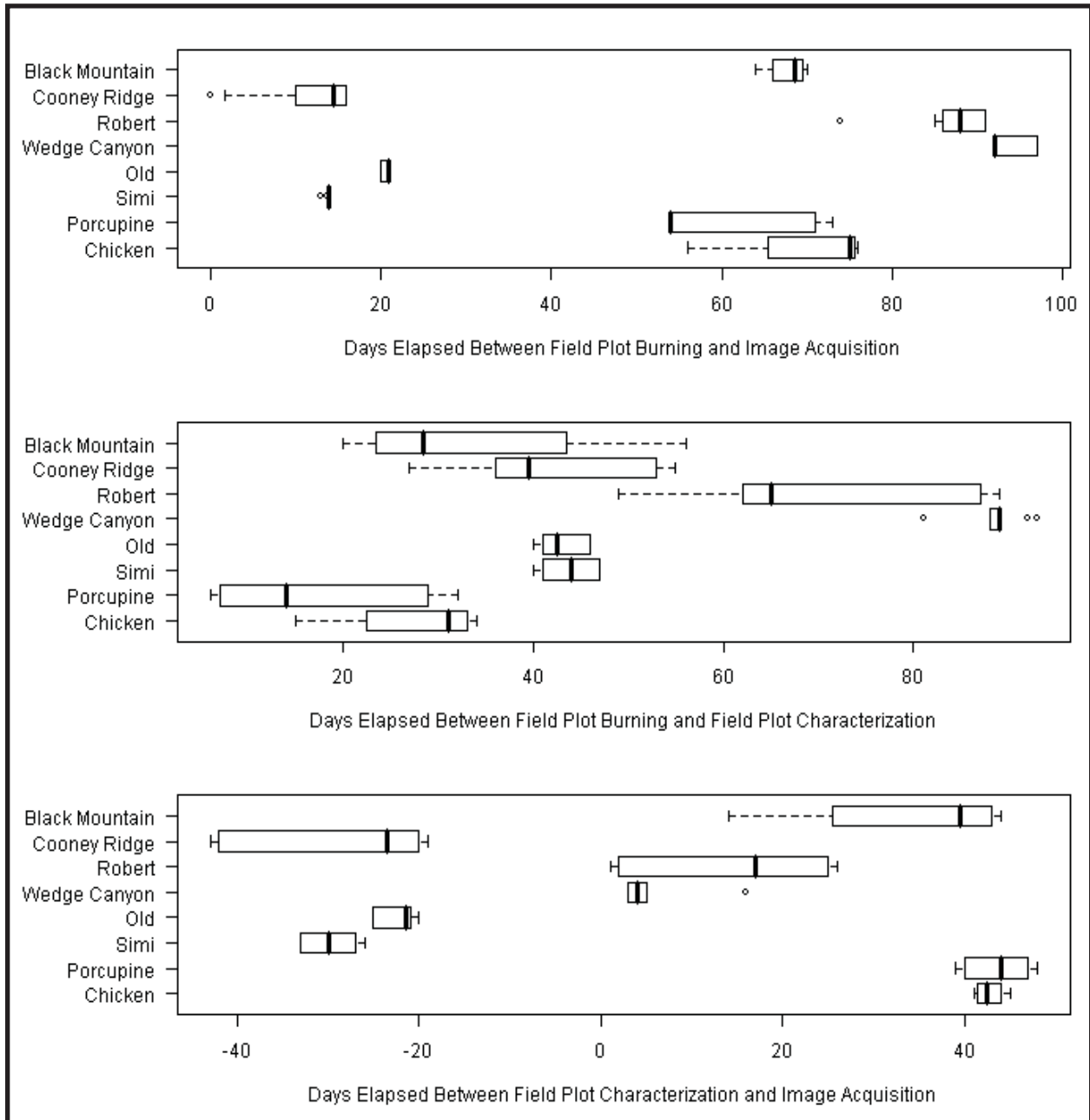


Figure 3. Boxplots of time lags between burn date, image acquisition date, and field characterization date, calculated for the field plots on the eight wildfires sampled. Thick vertical lines show the medians, box ends represent lower and upper quartiles, the line ends indicate the 5th and 95th percentiles, and dots farther out are outliers.

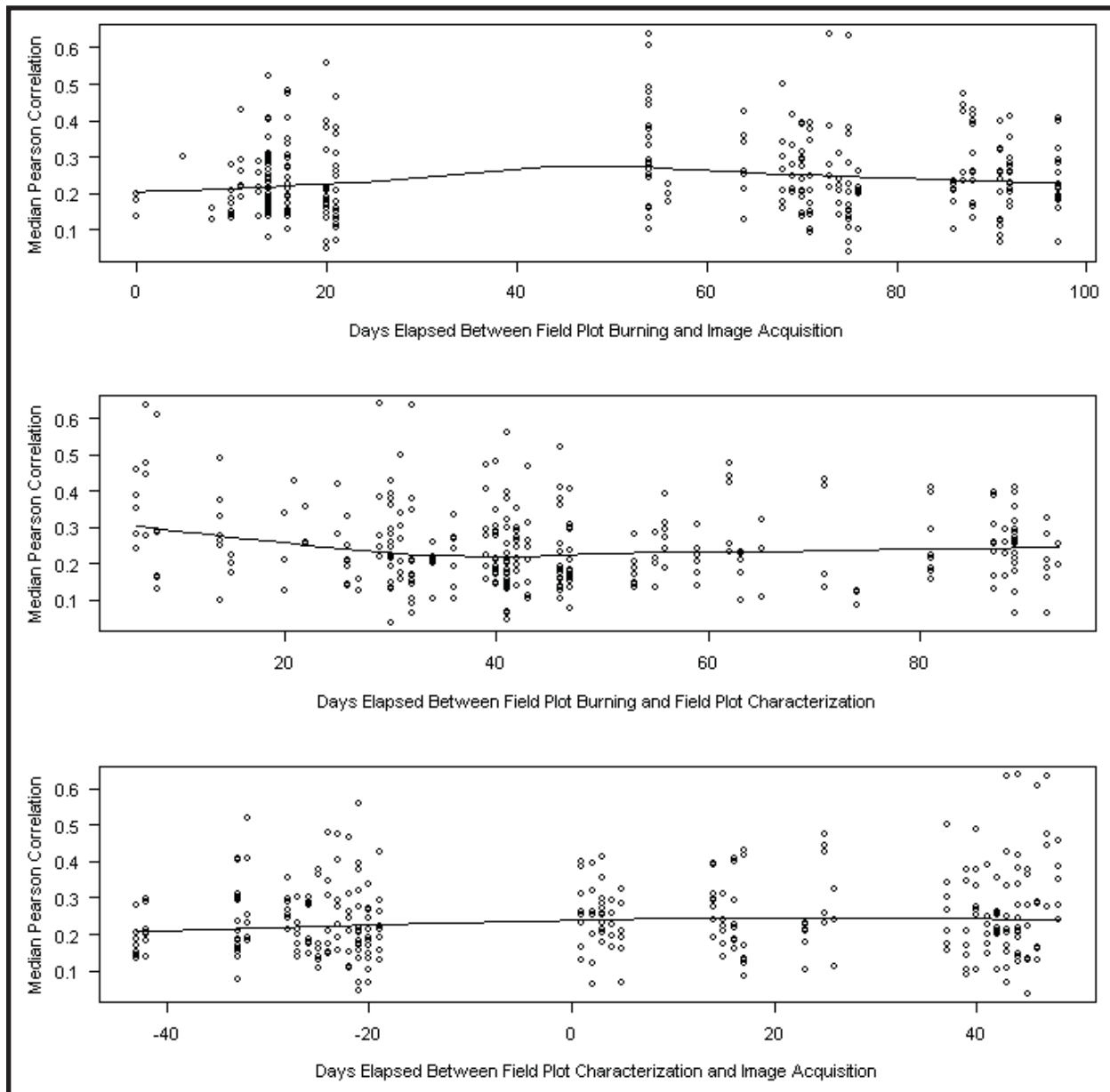


Figure 4. Scatterplots of time lags between burn date, image acquisition date, and field characterization date, versus the median of the Pearson correlations (absolute values) between the 8 image variables and 14 subplot-level surface cover fractions within the field plots. Smoothed loess fit lines are plotted to illustrate the trends.

Image Indices

The distributions of correlations between the eight Landsat 5 TM image-derived variables and 32 fire effects measures from the field varied somewhat between the eight wildfires sampled, but were usually fairly similar when compared across the eight image variables (Figure 5). When the correlation matrices from the Montana, California, and Alaska regions

were combined, so that the three regions were apportioned equal weight despite their different plot counts, it became more evident that green fraction and NBR performed best across these three very different ecosystems (Figure 6). Green fraction was more highly correlated to NBR than any of the other image indices in Montana ($r = 0.82$), California ($r = 0.63$), and Alaska ($r = 0.86$).

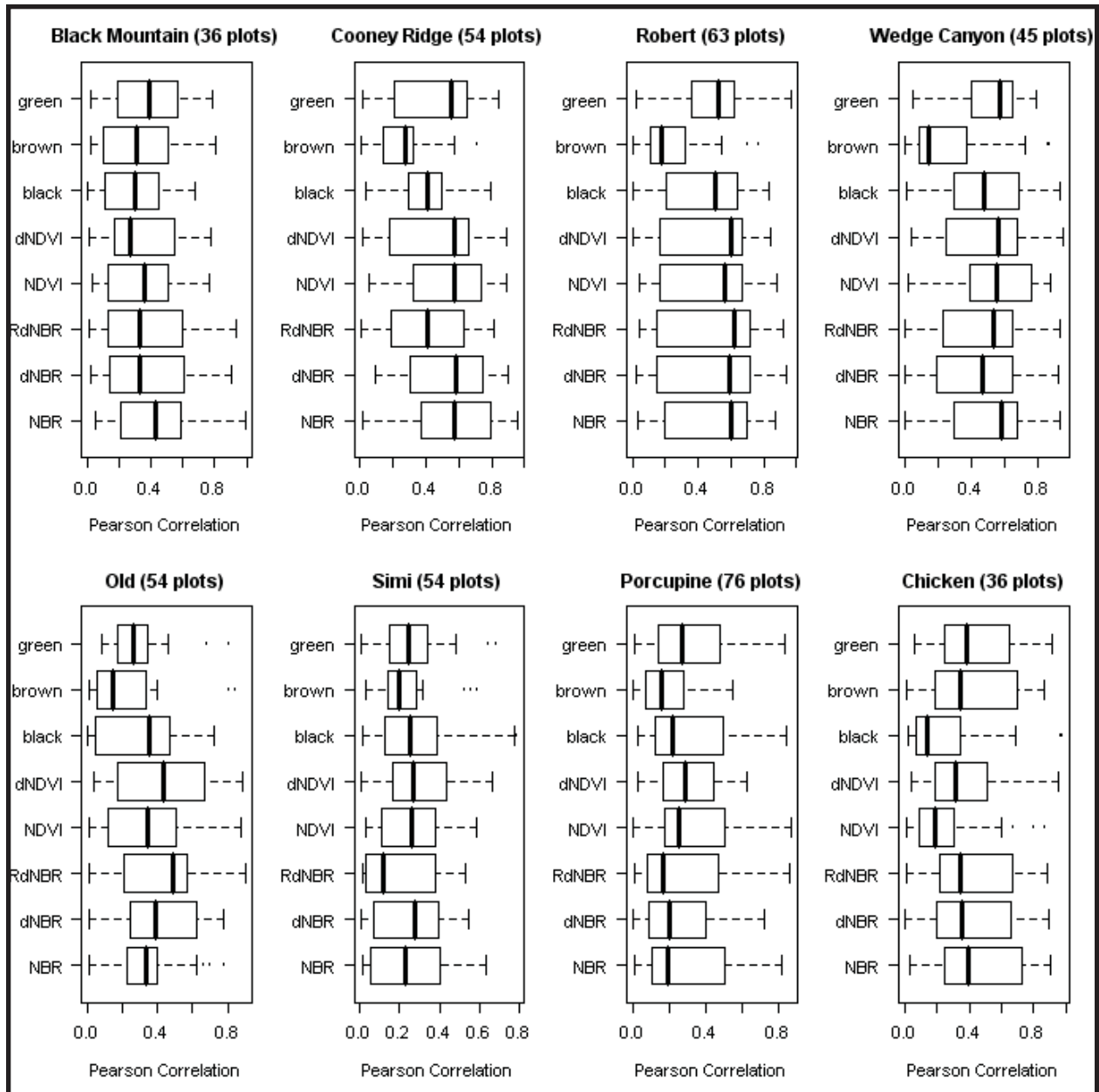


Figure 5. Boxplots of Pearson correlations (absolute values) between 32 field measures of fire effects and the eight Landsat image variables listed on the y-axes, partitioned according to the eight wildfires sampled.

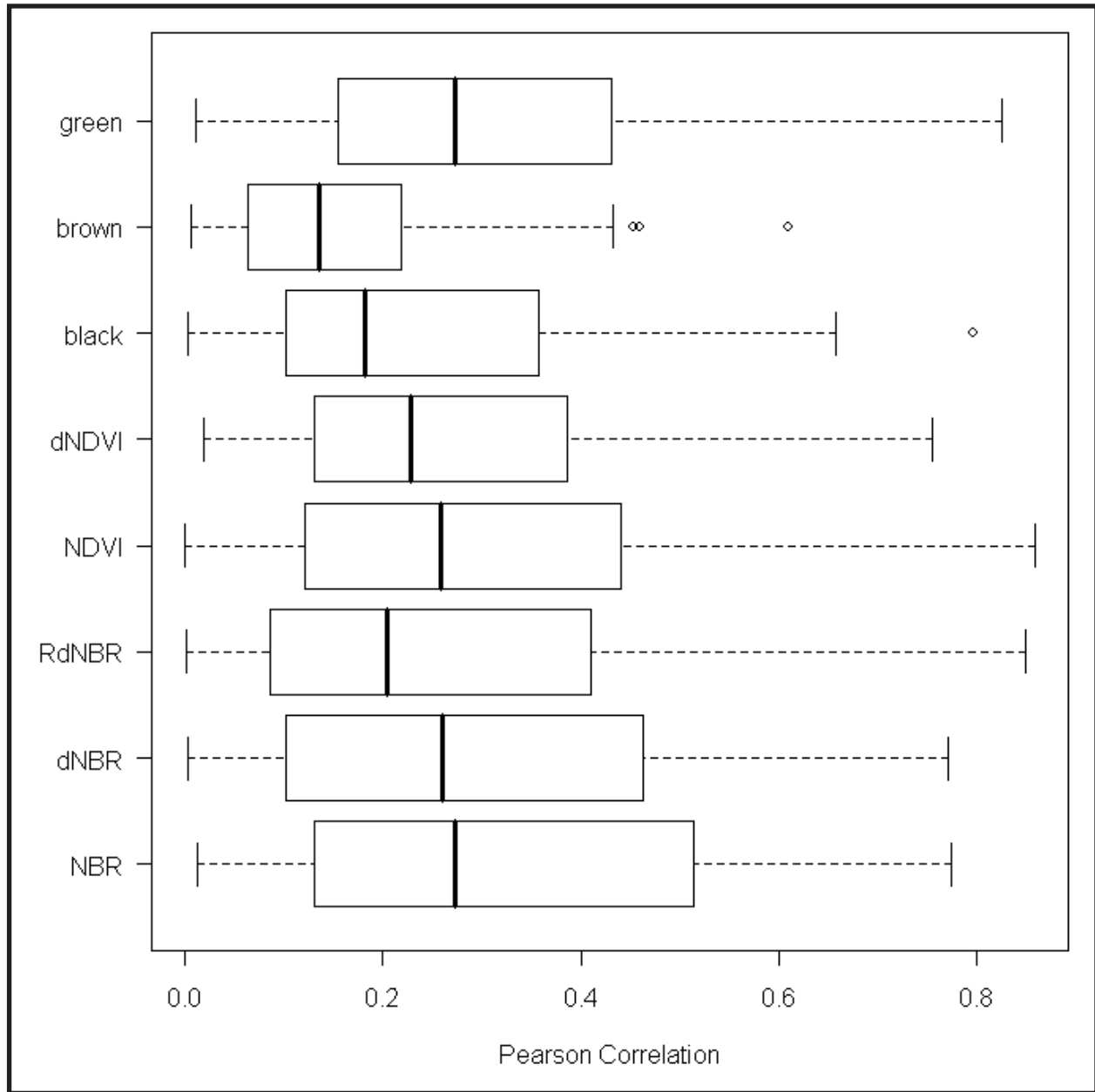


Figure 6. Boxplots of Pearson correlations (absolute values) between 32 field measures of fire effects and the eight Landsat image variables listed on the y-axis, calculated across all plots in each of the western Montana, southern California, and interior Alaska regions and then combined to represent the three regions equally.

In every region we sampled, we had the advantage of possessing another image from an alternative satellite acquired within a day of the Landsat 5 TM imagery used for the bulk of our analysis. At the Cooney Ridge fire, we compared NBR calculated from the Landsat 5 image to NBR calculated from a 1 Sep 2003 SPOT 4 image acquired the next day. A paired t-test showed that Landsat NBR did only insignificantly better ($p = 0.25$) than SPOT-derived NBR in terms of mean correlation strength to our 32 fire effects measures, although Landsat NDVI did significantly better ($p < 0.0001$) than SPOT NDVI, perhaps because the latter image appeared more smoky. We repeated these statistical tests at the Old fire, where an 18 Nov 2003 ASTER image was acquired one day prior to the Landsat 5 image. Here, the mean correlation strength of Landsat NBR to the 32 field measures was only negligibly higher ($p = 0.73$) than ASTER NBR, while ASTER NDVI did only negligibly better than Landsat NDVI ($p = 0.95$). Finally in Alaska, we took advantage of a 9 Sep 2004 Landsat 7 ETM+ image acquired one day after the Landsat 5 TM image to compare these two sensors. Fortunately, all of our field plots happened to be situated along the center of the ETM+ scene, the portion of the satellite path unaffected by the data gaps in ETM+ imagery since the 31 May 2003 failure of the scan line corrector (<http://landsat7.usgs.gov/updates.php>). We found Landsat 7 did significantly better than Landsat 5 using NBR ($p = 0.002$), but only negligibly better using NDVI ($p = 0.89$). Using a 3 Aug 2002 pre-fire ETM+ scene to also calculate differenced indices, we also found significant improvements using Landsat 7 dNBR ($p < 0.0001$) and RdNBR ($p = 0.0008$), but only insignificant improvement using Landsat 7 dNDVI ($p = 0.30$).

Fire Effects

The distributions of correlations between the 32 fire effects measures and the eight image

variables were highly variable when compared across the fire effects variables (Figures 7-9). No fire effects were consistently highly correlated to any of the image variables across all fires. The overstory measures of canopy closure, green and charred tree crowns were most highly correlated to the image variables in Montana, while understory measures were substantially less correlated (Figure 7). Old litter depth was more highly correlated to the image variables than other surface or subsurface measures, which varied widely in correlation strength (Figure 7).

The poorest correlations generally among the three regions sampled were observed in California (Figure 8). Trees were usually lacking in this predominantly chaparral vegetation, making tall shrub and sapling mortality the best vegetation correlates to the image variables. While still low, water repellency as measured by infiltrometer rate was better correlated to the image variables here than in Montana or Alaska (Figures 7-9), perhaps because the relative lack of vegetation and litter/duff cover in California exposed so much more soil here than in the other regions. However, spectral differentiation between the organic and inorganic surface components was poor (Figure 8).

In Alaska, canopy closure and green tree crown overstory measures, and understory tall shrubs, were more highly correlated to the image variables than were other vegetation measures (Figure 9). Charred and uncharred organics were correlated relatively well, as were total green, charred, and uncharred cover fractions, because little inorganic fraction existed to confuse the spectral reflectance signal in Alaska compared to Montana and California (Figs 7-9). The deep surface organic layer appears to be a more influential driver of spectral reflectance here in the black spruce forests of Alaska than in the ecosystems we sampled in Montana or California.

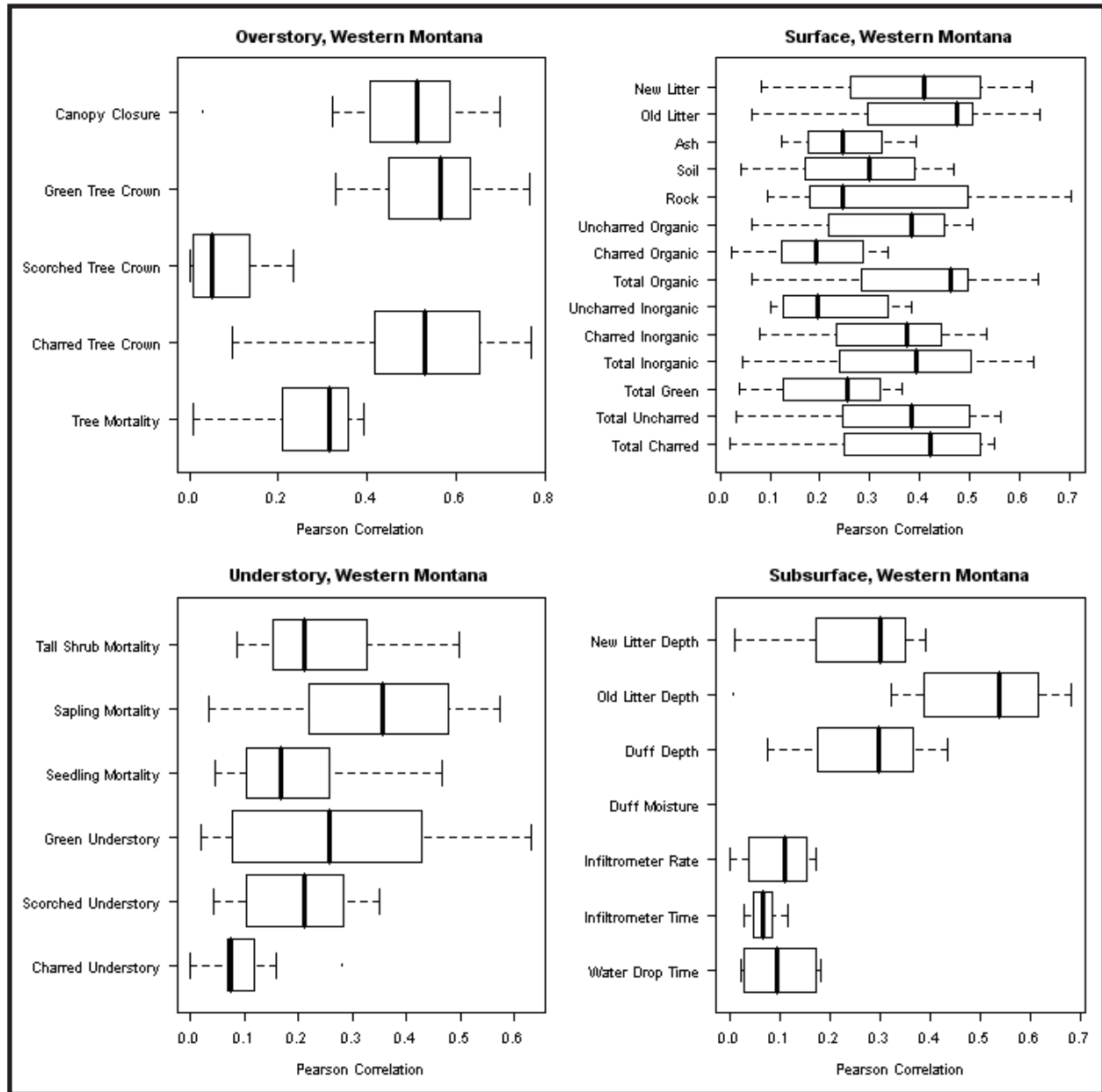


Figure 7. Boxplots of Pearson correlations (absolute values) between eight Landsat image variables of burn severity and 32 field measures of fire effects listed on the y axes, grouped into overstory, understory, surface, and subsurface variable categories, in western Montana.

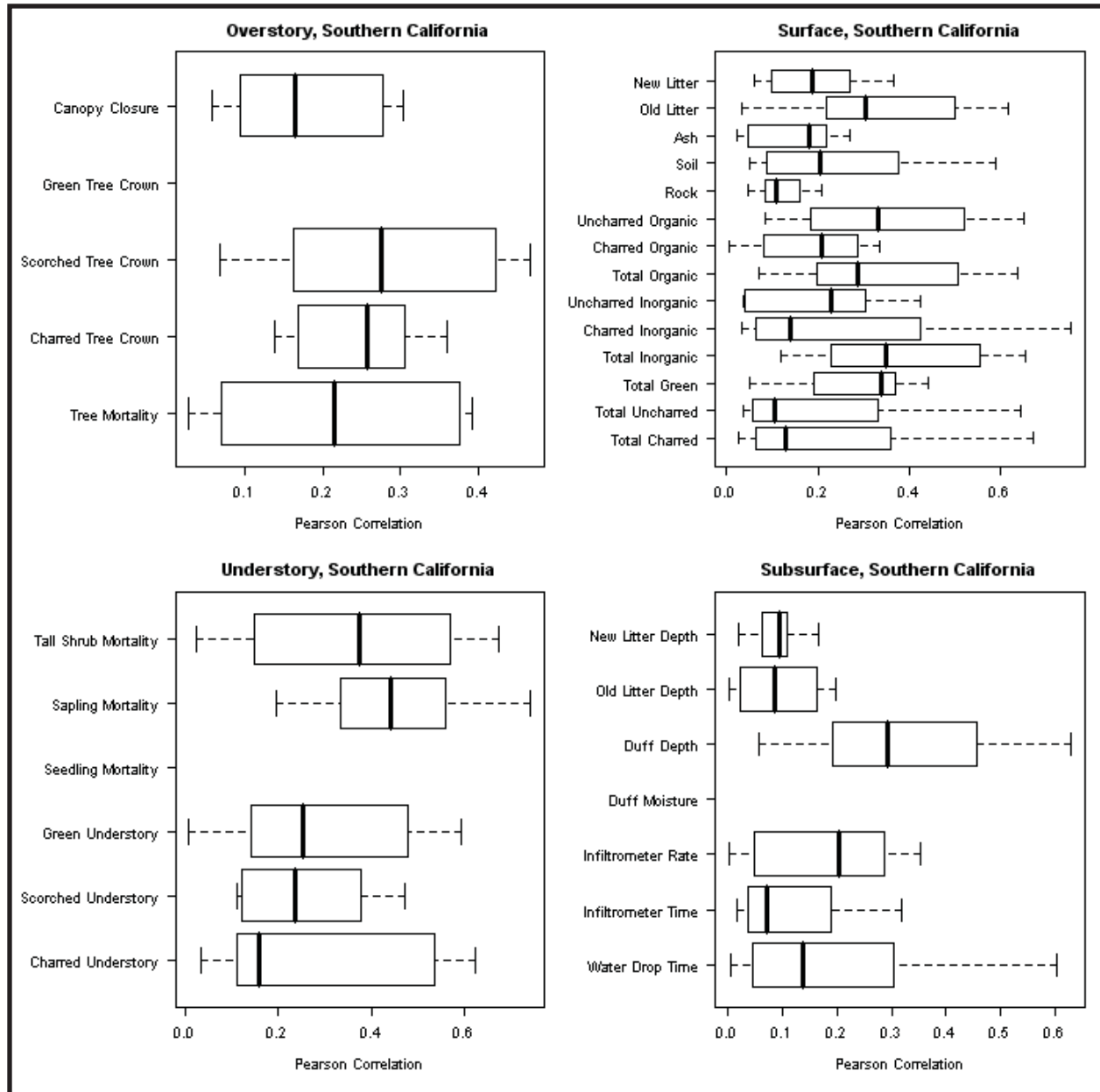


Figure 8. Boxplots of Pearson correlations (absolute values) between eight Landsat image variables of burn severity and 32 field measures of fire effects listed on the y axes, grouped into overstory, understory, surface, and subsurface variable categories, in southern California.

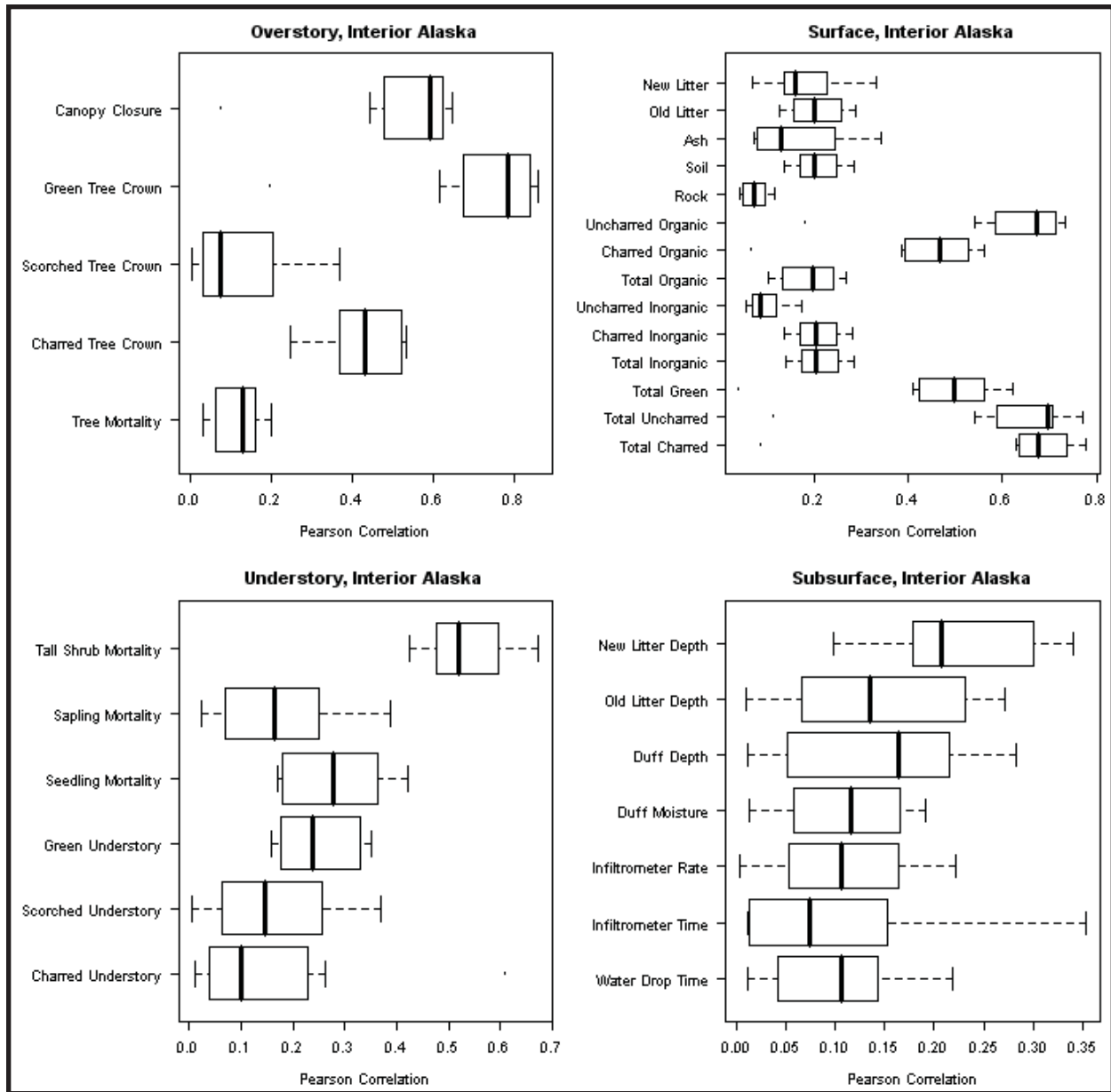


Figure 9. Boxplots of Pearson correlations (absolute values) between eight Landsat image variables of burn severity and 32 field measures of fire effects listed on the y axes, grouped into overstory, understory, surface, and subsurface variable categories, in interior Alaska.

We present more detailed results for exposed mineral soil cover, a measure of particular interest to BAER teams, to exemplify the high variability in observed fire effects between our selected study regions. Percent soil cover was twice as prevalent in California (68%) than in Montana (33%), while it comprised <9% of total surface cover in Alaska (Table 3). Although not

shown here, surface organic material followed the opposite trend. Aggregating the soil subplot measures to the plot and site levels improves the calculated correlations to the image variables by better capturing both the fine-scale (subpixel) variability in soil cover sampled on the ground, as well as the moderate-scale variability between pixels within the sampled burn severity

condition characterized by a field site (Figure 2). However, aggregation also reduces the sample size (N), hence producing fewer significant correlations at the plot scale, and fewest at the site scale. Spatial autocorrelation among subplots is biasing upwards the significance of the correlations computed at the subplot scale (Table 3).

DISCUSSION

Rapid Response

Satellite Measures. Landsat images were often not immediately available when BAER teams on the ground had critical need for BARC maps. SPOT imagery was used for BARC maps at the Montana fires. Coarse-resolution MODIS imagery was first used at the California fires, which was later supplanted by a higher-resolution MASTER (airborne) image at the Simi fire, and an ASTER image at the Old fire (Clark *et al.* 2003). Our consideration of alternative satellite sensors besides Landsat in this analysis was warranted given that other sensors are used by RSAC and EROS for BARC mapping, and because the aging Landsat 5 and 7 satellites will inevitably fail like their

predecessors, which is likely to precede the successful launch of a replacement from the Landsat Data Continuity Mission (<http://ldcm.nasa.gov>).

The SPOT 4 and 5 satellites have a SWIR band4(1580-1750nm)thatcloselyapproximates Landsat SWIR band 5 (1550-1750 nm), rather than the Landsat SWIR band 7 (2080-2350 nm) preferred for calculating NBR (Equation 1). In theory, the SPOT SWIR band 4 may be less useful for burn severity mapping using NBR than Landsat band 7 (Key and Benson 2003). However, our comparison in Montana could neither confirm nor refute this theory. Results from our comparison of Landsat TM to ASTER in California were similarly equivocal. In this case, the ASTER SWIR band 6 (2185-2225 nm) very closely approximates Landsat SWIR band 7. Our effective weighting of pixel proportions while aggregating the subplot-level data to the plot level may have negated the advantage of slightly higher spatial resolution of SPOT (20 m) and ASTER (15 m) imagery relative to Landsat (30 m). We attribute our slightly better Landsat 7 ETM+ results in Alaska to the improved radiometric resolution and less degraded condition of the ETM+ sensor compared to Landsat 5 TM.

Table 3. Mean and standard error of exposed mineral soil (%) sampled in subplots in three regions, and correlations to eight image variables aggregated to the site or plot levels, or not at all (subplot level). Significant pearson correlations ($\alpha = 0.05$) Are indicated in boldface.

Region	%Soil \pm SE	Scale	N	NBR	dNBR	RdNBR	NDVI	dNDVI	Black	Brown	Green
Montana											
		site	22	-0.587	0.368	0.275	-0.535	0.176	0.412	0.062	-0.539
		plot	198	-0.468	0.309	0.194	-0.422	0.147	0.291	0.041	-0.362
	32.8 \pm 0.6	subplot	2970	-0.382	0.249	0.157	-0.346	0.120	0.241	0.031	-0.295
California											
		site	12	-0.248	0.721	0.489	-0.344	0.789	0.083	0.132	-0.212
		plot	108	-0.161	0.493	0.251	-0.261	0.589	0.049	0.066	-0.110
	68.2 \pm 0.7	subplot	1620	-0.127	0.388	0.185	-0.207	0.467	0.047	0.049	-0.088
Alaska											
		site	16	-0.289	0.305	0.233	-0.326	0.378	0.209	0.364	-0.418
		plot	112	-0.184	0.228	0.136	-0.213	0.283	0.156	0.184	-0.262
	8.6 \pm 0.5	subplot	1680	-0.135	0.172	0.102	-0.165	0.217	0.120	0.131	-0.195

Field Measures. Fire effects can change quickly. Ash cover in particular is rapidly redistributed by wind and rainfall, which may largely explain why it was a consistently poor correlate to the image variables (Figures 7-9). Needlecast (new litter) on moderate severity sites is another dynamic phenomenon, as is green vegetation regrowth. In only two weeks post fire, bear grass appeared in Montana; manzanita, chamise, and other chaparral shrubs sprouted in California; and fireweed sprouted in Alaska and Montana. We made every effort to characterize our field sites as quickly after burning as was safely possible, but at a rate of one field site characterized per day, plus travel time just to get to the fire, it proved difficult to complete the fieldwork at each fire before weather and vegetation recovery had altered the post-fire scene. The plot-level correlation strength between image and field data did diminish slightly in the first 36 days following a fire (Figure 4). This addressed a concern expressed by Hudak *et al.* (2004b) over fire effects changing before they can be characterized in the field, but the weakness of the visible trend (Figure 4) alleviates this concern since it is apparently not an overriding factor.

Another consideration with this rapid response research project was the difficulty in objectively sampling the full range of fire effects during an active fire. Since the fire perimeter was still expanding, so were the proportions of burn severity classes upon which we might base a preliminary stratification for objectively selecting field sites. Furthermore, Incident Commanders are understandably uncomfortable allowing a research team to work too closely to the active fire front, which further limits options. These constraints necessitated a higher level of subjectivity in selecting sites relative to a typical landscape-level study. For these reasons, we strove to sample as wide a range of severity conditions as we could safely access, while also placing the

field site randomly within a chosen condition to limit potential sampling bias.

Burn Severity Indices

Several other indices were tested in a preliminary analysis of this same dataset (Hudak *et al.* 2006) but were excluded from the results presented in this paper because they were unhelpful. Hudak *et al.* (2006) found that neither the Enhanced Vegetation Index (EVI) (Huete *et al.* 2002) nor differenced EVI performed significantly better than the NBR or dNBR, respectively. Hudak *et al.* (2006) also tested three mathematical manipulations of the NBR that include the Landsat thermal band 6 (Holden *et al.* 2005), along with their respective differenced indices, but these also performed no better than simple NBR and dNBR (Hudak *et al.* 2006).

Hudak *et al.* (2006) found the NBR and NDVI indices outperformed their corresponding differenced indices, as well as RdNBR, at the Montana and Alaska fires. In contrast, the differenced indices performed better at the California fires. We examined our dataset in greater detail by partitioning the results by individual fires (Figure 5), but the same general conclusions held. The RdNBR performed best at the Old fire in California, which among the vegetation types we sampled was probably most similar structurally to the vegetation in the Sierra Nevada where RdNBR was successfully applied (Miller and Thode 2007). However, few differences between burn severity indices were significant at any of the fires (Figure 3), which was our rationale for combining the correlation matrices from the Montana, California, and Alaska regions to assess which indices best correlated to fire effects over these very different ecosystems (Figure 6).

The NBR index currently used by RSAC and EROS may be more satisfactory than NDVI, not because it performed negligibly

better in our broad analysis (Figure 6), but because the SWIR band used in the NBR formula (Equation 1) is less vulnerable to the scattering effects of smoke and haze than the RED band used to calculate NDVI (Equation 4). On the other hand, NDVI did not perform significantly worse than NBR, meaning NDVI could be substituted for NBR if, for example, Landsat or other imagery with a SWIR band are unavailable, as is often true for rapid response.

By default, RSAC and EROS use the dNBR to produce BARC maps. Key and Benson (2003) found several advantages of dNBR over NBR for extended burn severity assessment: better visual contrast, broader range of severity levels, and sharper delineation of the fire footprint. The influence of immediate fire effects on pixel reflectance attenuates over time, so including a pre-fire image to map the magnitude of change in the scene can be advantageous over simply mapping post-fire condition (Hudak and Brockett 2004, Hudak *et al.* 2007). On the other hand, the dates of pre- and post-fire images selected to produce differenced indices are often offset by several weeks; such mismatches cause inconsistencies in sun angle and vegetation phenology that add undesired variation to differenced indices and can limit their utility (Key 2006). In general, our results suggest that for BARC maps used for preliminary burn severity assessments, NBR may be preferable to dNBR. RSAC and EROS currently produce and archive pre-fire NBR, post-fire NBR, and dNBR products, which we consider as sensible practice given all these considerations.

Fire Effects

Green vegetation had more influence on the image variables than any other surface constituent (Figures 5-9). In other words, burn severity as indicated in BARC maps is more sensitive to vegetation effects than soil effects, so we caution against interpreting BARC maps

as burn severity maps, particularly in terms of soil severity (Parsons and Orlemann 2002) without the field verification that BAER teams often do to improve their interpretation of burn severity from these maps. It should be expected that indices derived from a satellite image overhead would correlate better with vegetation than with soil characteristics because vegetation occludes the ground. Percent soil cover was most highly correlated to NBR in Montana and to dNDVI in California and Alaska (Table 3). The strength of these correlations corresponded with the degree of soil exposure: strongest in California, less strong in Montana, and weakest in Alaska. Similarly, surface organic materials that protect the soil were more prevalent in Alaska than in Montana or especially California, again matching the trend in their correlation strength to the image variables (Figures 7-9). We also found burn severity indices generally correlated better to surface variables than soil water repellency variables (Figures 7-9), since surface reflectance should be more correlated to surface characteristics than to soil processes measured beneath the surface.

Hudak *et al.* (2004a) used semivariograms to show that fire effects can vary greatly across multiple spatial scales ranging from the 2-m sampling interval between adjacent subplots to the 130-m span of an entire field site (Figure 2). Our study supports earlier evidence that fire effects are more heterogeneous on low and moderate severity sites than on high severity sites (Turner *et al.* 1999). This helps explain why higher severity sites are more accurately classified on BARC maps than lower severity sites (Bobbe *et al.* 2003). Observed pixel reflectance is a function of all of the constituents occurring within that pixel, and to a lesser degree its neighboring pixels. Thus an image index of burn severity should not be expected to correlate very well with any single fire effect measured on the ground, when pixel reflectance is a function of multiple fire effects.

Pixels are fundamentally mixed, which is strong justification for pursuing spectral mixture analysis (SMA) as a more robust strategy for mapping fire effects. The green, brown, and black variables included with the five burn severity indices in our analysis (Figures 5-6) represent green vegetation, dead or nonphotosynthetic vegetation, and char fractional cover, respectively, estimated via SMA. The six multispectral bands of Landsat TM images are not nearly as suited for SMA as hyperspectral images, but sufficient for differentiating green and possibly char cover fractions. Our green fractional cover estimate performed as well as NBR (Figures 5-6), among the burn severity indices tested. Perhaps most importantly, an image of estimated green vegetation cover has direct biophysical meaning, unlike NBR or other band ratio index. Importantly, calculation of the green (and other) fractions by spectral mixture analysis does not rely on the inclusion of all six Landsat bands. In the event that imagery is only available with the spectral equivalent of say, Landsat bands 1-4, these cover fractions could still be produced, whereas the NBR could not. Our inclusion of the green, brown, and black fractional cover estimates is instructive as it suggests that the five burn severity indices tested correspond more closely to green and black fractions than to brown fraction, the poorest correlate to measured fire effects. Unlike ash cover, char fraction remains relatively intact in the post-fire scene, and might be a suitable biophysical variable upon which to base a burn severity map derived using SMA. Green and char cover fractions correlated with fire effects as well as many of the burn severity indices tested (Figures 5-6), so fractional cover maps could be at least as useful to BAER teams as the current NBR- or dNBR-based BARC maps. For instance, it would be more difficult to misconstrue a char cover fraction map (labeled as such) as a soil severity map, as NBR- or dNBR-based BARC maps have been misinterpreted (Parsons and Orlemann 2002). An added advantage of

mapping fractional cover estimates is that they represent remote analogues to the traditional field 'severity' measures of percent green, brown, and black (Lentile *et al.* 2006).

An important consideration not conveyed in Figures 7-9 is the tremendous variation in inorganic and organic surface cover fractions observed in this study both within and between study regions. Lentile *et al.* (2007) detail the variability in ash, soil, and surface organics in each region and across low, moderate, and high severity burn classes. Ash cover was highest in Montana, soil cover highest in California, and surface organics highest in Alaska. The broader reach of the boxplots in Figures 7-8 compared to Figure 9 is in large part due to greater variability in inorganic and organic cover fractions in Montana and California than in Alaska, where much of the organic matter persists even after a severe burn. Conversely, little soil was exposed in Alaska compared to Montana or especially California. We tested whether correlations between percent soil and the image variables were higher on high severity sites. Generally they were not, except in Alaska, because so little soil was exposed except on high severity sites (Lentile *et al.* 2007). Summarizing all of the fire effects measured in the field is not essential for communicating the image-field data relationships central to this paper, yet it is helpful to remember that sampling a wide range of variability in fire effects in the field is essential for understanding the influence any of them may have on pixel reflectance. Similarly, closely spaced samples (such as our subplots) are essential for capturing subpixel, fine-scale variability.

We chose percent exposed mineral soil, probably the most important fire effects measure to BAER teams (H. Shovic, personal communication), to further illustrate this scaling issue (Table 3). When percent soil is correlated to pixel values at the fundamental subplot scale, often only 1 or at most 4 Landsat TM pixels will be sampled in a single 9 m x 9 m plot. The significance tests at the subplot scale

have unreliably inflated degrees of freedom stemming from spatial autocorrelation, because the same image pixels get oversampled by the closely spaced subplots. On the other hand, the significance tests at the plot scale are reliable because plots A-I are spaced far enough apart to ensure that different image pixels get sampled (Figure 2), although this does not completely eliminate potential autocorrelation effects (Hudak *et al.* 2004a). Aggregating the field and image data at the 15 subplots to the plot level invariably improves the correlations (Table 3), with the multiple subplot locations providing appropriate weight to the image pixel values being aggregated. Further aggregation to the site scale further improves the correlations because that much more variation gets sampled (Table 3). This same pattern can be observed for the other fire effects sampled under our spatially nested design (Figure 2). Even if image georegistration was perfect, the field validation data could relate poorly to the image data because widely separated points only sample single pixels in the image subject to validation, and single points are not very representative of image pixel values if the field variables of interest vary greatly at subpixel scales.

The downside of nested sampling designs such as ours is fewer field sites get sampled across the landscape because so much time is required to characterize a field site comprised of multiple plots and subplots. To speed sampling, we only used one set of nested plots to sample vegetation overstory and understory variables (Figure 2) because we reasoned these would not require the same sampling effort to achieve reasonably good correlations to the image variables as with the surface and subsurface variables (Table 2). This proved to be the case because of our rule that the field site center, although randomly placed, should not be placed too closely to an edge in the severity condition observed in the field. This ensured that the center image pixel to be correlated with the overstory and understory variables was representative of the entire field site. We

did not aggregate our data to the site scale for the bulk of our analysis (Figures 5-9) because that would have left too few sample units upon which to base the correlations, especially at the level of individual wildfires (Figure 5). In summary, our hierarchical sampling strategy is not recommended for BAER teams or others who require rapid response or rapid results. It was designed specifically to explore and exploit the spatial autocorrelation that underlies observed patterns in fire effects.

While a soil fractional cover map would be very useful to BAER teams, spectra for most soil types would be well mixed with the spectra for surface litter and nonphotosynthetic vegetation, and difficult to differentiate with 6-band multispectral Landsat data. Soil types varied greatly within and between our sample sites, making application of a single, generic soil endmember untenable. A spectral library of endmember spectra for specific soil types is available online from USGS (<http://speclab.cr.usgs.gov/spectral-lib.html>). We used a field spectroradiometer (ASD FieldSpec Pro FR) to gather endmember spectra of soils, char, ash, litter, nonphotosynthetic vegetation, and the major plant species at the wildfires we sampled; a spectral library of these endmembers is also available online (http://frames.nbii.gov/portal/server.pt?open=512&objID=500&mode=2&in_hi_userid=2&cached=true). We also obtained airborne hyperspectral imagery over all of our field sites in the eight wildfires sampled to test more rigorously whether maps of green, char, soil, or other cover fractions derived from spectral mixture analysis could potentially replace current burn severity maps based on indices (Lewis *et al.* 2007). The 4 m to 5 m spatial resolution of our hyperspectral imagery will allow more rigorous assessment of the tremendous spatial heterogeneity occurring at subpixel scales. Our spatially nested field data will serve as valuable ground truth for validating estimates of multiple cover fractions derived from spectral mixture analysis.

CONCLUSIONS

Our results show that the NBR and dNBR burn severity indices, as are currently used in BARC maps of large wildfires in the United States, are sound choices for rapid, preliminary assessment of immediate post-fire burn severity across different ecosystems. We recommend that RSAC and EROS continue their current practice of archiving the continuous NBR and dNBR layers upon which BARC maps are based, for future retrospective studies. The correlations of NDVI and dNDVI to the same suite of 32 fire effects measures generally were not significantly worse, so these indices could serve as suitable substitutes for NBR and dNBR. This result is highly relevant to the Monitoring Trends in Burn Severity project (MTBS), a multi-year effort by RSAC and EROS to map the burn severity and perimeters of fires across the entire United States from 1984 through 2010 (<http://svinetfc4.fs.fed.us/mtbs>). The MTBS project should consider extending their historical scope and map burn severity and perimeters of fires preceding the availability of Landsat TM imagery, using the 1972-84 Landsat Multispectral Scanner (MSS) image record and dNDVI, since MSS images lack the SWIR band needed to calculate dNBR. In this study, the RdNBR only produced better correlations to fire effects at one of the eight wildfires sampled; thus, it may have more limited broad-scale utility. Time and money limited our sampling to only three regions, but it is difficult to imagine three ecosystems that could be more representative of the diverse fire ecology in North America than the three we selected in western Montana, southern California, and interior Alaska.

Our results show high variability in the relationships between indices derived from satellite imagery and fire effects measured on the ground, yet some remarkable consistencies across the three ecosystems sampled. First,

none of the indices were very highly correlated with any of the 32 specific fire effects measured, which is likely a reflection of the 30 m scale of Landsat data relative to the finer scale at which fire effects vary. Second, the uppermost vegetation layers (trees in Montana and Alaska, shrubs in California) had more influence on the image indices than surface vegetation. Likewise, major surface cover fractions were better correlated to the image indices than minor surface cover fractions or subsurface measures of soil water repellency. BAER teams should consider BARC maps much more indicative of post-fire vegetation condition than soil condition, and factor in that awareness when validating BARC maps on the ground. In terms of soil effects, BARC maps are more likely to be inaccurate on low or moderate severity sites than on high severity sites, where less vegetation remains to obstruct the view of the soil condition from above, as in an image. This conclusion is useful to BAER teams primarily interested in severe soil effects with little protective overhead vegetation cover.

By definition, burn severity is a measure of the ecological changes wrought by fire. Understory vegetation response (Lentile *et al.* 2007, and references therein), potential for soil erosion, and probable effects on soil nutrients are all more pronounced where fires have consumed more fuel and resulted in more mineral soil exposure. Our results demonstrate that image spectral reflectance upon which indices are based is largely a function of the proportions of surface materials comprising the scene. Our future research will focus on spectral mixture analysis of hyperspectral imagery. We think this approach acknowledges that pixel reflectance is fundamentally a mixture of charred, dead, nonphotosynthetic and green vegetation, soil, rock and ash materials that vary greatly at fine scales.

ACKNOWLEDGMENTS

This research was supported in part by funds provided by the Rocky Mountain Research Station, Forest Service, U.S. Department of Agriculture (Research Joint Venture Agreement 03-JV-111222065-279), the USDA/USDI Joint Fire Science Program (JFSP 03-2-1-02), and the University of Idaho. Randy McKinley performed this work under USGS contract 03CRCN0001. Carter Stone, Stephanie Jenkins, Bryn Parker, K.C. Murdock, Kate Schneider, Jared Yost, Troy Hensiek, Jon Sandquist, Don Shipton, Jim Hedgecock, and Scott MacDonald assisted with field data collection, and Jacob Young and Curtis Kvamme with data entry. The GIS work was facilitated by an AML routine written by Jeff Evans. We appreciate the help of local natural resources managers in each location, as well as the incident management teams. We thank RMRS statistician R. King, USGS editor K. Nelson, and three anonymous reviewers for their constructive comments.

LITERATURE CITED

- Barbosa, P.M., J.-M. Grégoire and J.M.C. Pereira. 1999. An algorithm for extracting burned areas from time series of AVHRR GAC data applied at a continental scale. *Remote Sensing of Environment* 69: 253-263.
- Bobbe, T., M.V. Finco, B. Quayle, K. Lannom, R. Sohlberg and A. Parsons. 2003. Field measurements for the training and validation of burn severity maps from spaceborne, remotely sensed imagery. Final Project Report, Joint Fire Science Program-2001-2, 15 p.
- Clark, J., A. Parsons, T. Zajkowski and K. Lannom. 2003. Remote sensing imagery support for Burned Area Emergency Response teams on 2003 southern California wildfires. USFS Remote Sensing Applications Center BAER Support Summary, 25 p.
- Cochrane, M.A. and C.M. Souza. 1998. Linear mixture model classification of burned forests in the Eastern Amazon. *International Journal of Remote Sensing* 19: 3433-3440.
- DeBano, L.F. 1981. Water repellent soils: A state of art. General Technical Report PSW-46. Berkeley, CA: USDA Forest service General Technical Report PSW-46.
- Elvidge, C.D. 1990. Visible and near infrared reflectance characteristics of dry plant materials, *International Journal of Remote Sensing* 11: 1775-1795.
- Gregoire, J.-M., K. Tansey and J.M.N. Silva. 2003. The GBA2000 initiative developing a global burnt area database from SPOT-VEGETATION imagery. *International Journal of Remote Sensing* 24: 1369-1376.
- Holden, Z.A., A.M.S. Smith, P. Morgan, M.G. Rollins and P.E. Gessler. 2005. Evaluation of novel thermally enhanced spectral indices for mapping fire perimeters and comparisons with fire atlas data. *International Journal of Remote Sensing* 26: 4801-4808.
- Hudak, A.T. and B.H. Hudak, A.T., and B.H. Brockett. 2004. Mapping fire scars in a southern African savannah using Landsat imagery. *International Journal of Remote Sensing* 25: 3231-3243.
- Hudak, A., P. Morgan, C. Stone, P. Robichaud, T. Jain and J. Clark. 2004a. The relationship of field burn severity measures to satellite-derived Burned Area Reflectance Classification (BARC) maps. Pages 96-104 in: American Society for Photogrammetry and Remote Sensing Annual Conference Proceedings, CD-ROM.

- Hudak, A., P. Robichaud, J. Evans, J. Clark, K. Lannom, P. Morgan and C. Stone. 2004b. Field validation of Burned Area Reflectance Classification (BARC) products for post fire assessment. Proceedings of the Tenth Biennial Forest Service Remote Sensing Applications Conference, CD-ROM.
- Hudak, A.T., S. Lewis, P. Robichaud, P. Morgan, M. Bobbitt, L. Lentile, A. Smith, Z. Holden, J. Clark and R. McKinley. 2006. Sensitivity of Landsat image-derived burn severity indices to immediate post-fire effects. 3rd International Fire Ecology and Management Congress Proceedings, CD-ROM.
- Hudak, A.T., P. Morgan, M. Bobbitt and L. Lentile. 2007. Characterizing stand-replacing harvest and fire disturbance patches in a forested landscape: A case study from Cooney Ridge, Montana. In *Understanding Forest Disturbance and Spatial Patterns: Remote Sensing and GIS Approaches*, edited by M.A. Wulder and S.E. Franklin, 209-231. Taylor & Francis, London.
- Huete, A., K. Didan, T. Muiira, E.P. Rodriguez, X. Gao and L.G. Ferreira. 2002. Overview of the radiometric and biophysical performance of the MODIS vegetation indices. *Remote Sensing of Environment* 83: 195-213.
- Key, C.H. and N.C. Benson. 2003. The Normalized Burn Ratio, a Landsat TM radiometric index of burn severity. <http://nrmssc.usgs.gov/research/ndbr.htm>.
- Key, C.H. 2006. Ecological and sampling constraints on defining landscape fire severity. *Fire Ecology* 2(2): 34-59.
- Landmann, T. 2003. Characterizing sub-pixel Landsat ETM+ fire severity on experimental fires in the Kruger National Park, South Africa. *South Africa Journal of Science* 99: 357-360.
- Lentile, L.B., Z.A. Holden, A.M.S. Smith, M.J. Falkowski, A.T. Hudak, P. Morgan, S.A. Lewis, P.E. Gessler and N.C. Benson. 2006. Remote sensing techniques to assess active fire characteristics and post-fire effects. *International Journal of Wildland Fire* 15: 319-345.
- Lentile, L.B., P. Morgan, C. Hardy, A. Hudak, R. Means, R. Ottmar, P. Robichaud, E. Kennedy Sutherland, J. Szymoniak, F. Way, J. Fites-Kaufman, S. Lewis, E. Mathews, H. Shovic and K. Ryan. 2007a. Value and challenges of conducting rapid response research on wildland fires. RMRS-GTR-193, 16 p.
- Lentile, L.B., P. Morgan, C. Hardy, A. Hudak, R. Means, R. Ottmar, P. Robichaud, E. Kennedy Sutherland, F. Way, S. Lewis. 2007b. Lessons learned from rapid response research on wildland fires. *Fire Management Today* 67: 24-31.
- Lentile, L.B., P. Morgan, A.T. Hudak, M.J. Bobbitt, S.A. Lewis, A.M.S. Smith and P.R. Robichaud. 2007. Burn severity and vegetation response following eight large wildfires across the western US. *Fire Ecology* 3(1): 91-108.
- Lewis, S.A., J.Q. Wu and P.R. Robichaud. 2006. Assessing burn severity and comparing soil water repellency, Hayman Fire, Colorado. *Hydrological Processes* 20: 1-16.
- Lewis, S.A., L.B. Lentile, A.T. Hudak, P.R. Robichaud, P. Morgan and M.J. Bobbitt. 2007. Mapping post-wildfire ground cover after the 2003 Simi and Old wildfires in southern California. *Fire Ecology* 3(1): 109-128.
- Miller, J.D. and A.E. Thode. 2007. Quantifying burn severity in a heterogeneous landscape with a relative version of the differenced Normalized Burn Ratio (dNBR). *Remote Sensing of Environment* 109: 66-80.
- Morgan, P., C.C. Hardy, T. Swetnam, M.G. Rollins and L.G. Long. 2001. Mapping fire regimes across time and space: Understanding coarse and fine-scale fire patterns. *International Journal of Wildland Fire* 10: 329-342.

- Morgan, P., G.E. Defosse and N.F. Rodriguez. 2003. Management implications of fire and climate changes in the western Americas. In *Fire and Climatic Change in Temperate Ecosystems of the Western Americas*, edited by T.T. Veblen, W.L. Baker, G. Montenegro, and T.W. Swetnam, 413-440. Ecological Studies 160. Springer-Verlag, New York.
- National Wildfire Coordination Group. 2005. Glossary of wildland fire terminology. US National Wildfire Coordination Group Report PMS-205. Ogden, UT.
- Parsons, A. and A. Orlemann. 2002. Burned Area Emergency Rehabilitation (BAER) / Emergency Stabilization and Rehabilitation (ESR). Burn Severity Definitions / Guidelines Draft Version 1.5, 27 p.
- Robichaud, P.R., D.S. Gasvoda, R.D. Hungerford, J. Bilskie, L.E. Ashmun and J. Reardon. 2004. Measuring duff moisture content in the field using a portable meter sensitive to dielectric permittivity. *International Journal of Wildland Fire* 13: 343-353.
- Robichaud, P.R., S.A. Lewis, D.Y.M. Laes, A.T. Hudak, R.F. Kokaly and J.A. Zamudio. 2007. Postfire soil burn severity mapping with hyperspectral image unmixing. *Remote Sensing of Environment* 108: 467-480.
- Robichaud, P.R., S.A. Lewis, and L.E. Ashmun. 2007. New procedure for sampling infiltration to assess post-fire soil water repellency. USDA Forest Service Research Note. RMRS-RN-32.
- Robinson, J.M. 1991. Fire from space: Global fire evaluation using infrared remote sensing. *International Journal of Remote Sensing* 12: 3-24.
- Smith, A.M.S., M.J. Wooster, A.K. Powell and D. Usher. 2002. Texture based feature extraction: application to burn scar detection in Earth Observation satellite imagery. *International Journal of Remote Sensing* 23: 1733-1739.
- Smith, A.M.S., M.J. Wooster, N.A. Drake, F.M. Dipotso, M.J. Falkowski and A.T. Hudak. 2005. Testing the potential of multi-spectral remote sensing for retrospectively estimating fire severity in African savannahs environments. *Remote Sensing of Environment* 97: 92-115.
- Smith, A.M.S., N.A. Drake, M.J. Wooster, A.T. Hudak, Z.A. Holden and C.J. Gibbons. 2007. Production of Landsat ETM+ reference imagery of burned areas within southern African savannahs: Comparison of methods and application to MODIS. *International Journal of Remote Sensing* 28: 2753-2775.
- Stroppiana, D., S. Pinnock, J.M.C. Pereira and J.-M. Gregoire. 2002. Radiometric analysis of SPOT-VEGETATION images for burnt area detection in Northern Australia. *Remote Sensing of Environment* 82: 21-37.
- Turner, M.G., W.H. Romme and R.H. Gardner. 1999. Prefire heterogeneity, fire severity, and early postfire plant reestablishment in subalpine forests of Yellowstone National Park, Wyoming. *International Journal of Wildland Fire* 9: 21-36.
- van Wagtenonk, J.W., R.R. Root and C.H. Key. 2004. Comparison of AVIRIS and Landsat ETM+ detection capabilities for burn severity. *Remote Sensing of Environment* 92: 397-408.
- Wessman, C.A., C.A. Bateson and T.L. Benning. 1997. Detecting fire and grazing patterns in tallgrass prairie using spectral mixture analysis. *Ecological Applications* 7: 493-511.
- Zhang, Y.-H., M.J. Wooster, O. Tutabalina and G.L.W. Perry. 2003. Monthly burned area and forest fire carbon emission estimates for the Russian Federation from SPOT VGT. *Remote Sensing of Environment* 87: 1-15.